Human Carbonic Anhydrase III: Structural and Kinetic Study of Catalysis and Proton Transfer[†,‡]

David M. Duda,[§] Chingkuang Tu,[||] S. Zoë Fisher,[§] Haiqain An,[||] Craig Yoshioka,[§] Lakshmanan Govindasamy,[§] Philip J. Laipis,[§] Mavis Agbandje-McKenna,[§] David N. Silverman,*[,||] and Robert McKenna*[,§]

Departments of Biochemistry and Molecular Biology and of Pharmacology and Therapeutics, College of Medicine, University of Florida, Gainesville, Florida 32610

Received April 1, 2005; Revised Manuscript Received June 3, 2005

ABSTRACT: The residue phenylalanine 198 (Phe 198) is a prominent cause of the lower activity of human carbonic anhydrase III (HCA III) compared with HCA II and other isozymes which have leucine at this site. We report the crystal structures of HCA III and the site-directed mutant F198L HCA III, both at 2.1 Å resolution, and the enhancement of catalytic activity by exogenous proton donors containing imidazole rings. Both enzymes had a hexahistidine extension at the carboxy-terminal end, used to aid in purification, that was ordered in the crystal structures bound in the active site cavity of an adjacent symmetry-related enzyme. This observation allowed us to comment on a number of possible binding sites for imidazole and derivatives as exogenous proton donors/acceptors in catalysis by HCA III. Kinetic and structural evidence indicates that the phenyl side chain of Phe 198 in HCA III, about 5 Å from the zinc, is a steric constriction in the active site, may cause altered interactions at the zinc-bound solvent, and is a binding site for the activation of catalysis by histidylhistidine. This suggests that sites of activation of the proton-transfer pathway in carbonic anhydrase are closer to the zinc than considered in previous studies.

Carbonic anhydrases are, with some exceptions, zinc-containing metalloenzymes that catalyze in two stages the hydration of CO_2 to HCO_3^- and a proton (*1*−*3*). The first stage in the hydration direction is the nucleophilic attack of the zinc-bound hydroxide on CO_2, followed by the dissociation of the resulting HCO_3^- from the zinc and the replacement of this ligand by water (eq 1). The second step regenerates the catalytically active zinc-bound hydroxide by a series of proton transfers (eq 2; *1*−*3*):

$$EZn{-}OH^- + CO_2 \leftrightarrows EZn{-}HCO_3^- \overset{H_2O}{\rightleftharpoons} EZn{-}H_2O + HCO_3^- \quad (1)$$

$$B + EZn{-}H_2O \leftrightarrows BH^+ + EZn{-}OH^- \quad (2)$$

where B represents an exogenous proton acceptor present in the bulk solvent. In human carbonic anhydrase II (HCA II)[1] the side chain of His 64, located about 7.5 Å from the zinc, acts as a proton shuttle in the transfer of protons between the active site and the bulk solvent during the catalyzed hydration (*1*−*6*).

The α class of carbonic anhydrases contains the mammalian enzymes including 14 known isozymes of human carbonic anhydrase with varying tissue distributions and catalytic activity (*1*, *7*, *8*). Human carbonic anhydrase III (HCA III) is cytosolic and is expressed at high levels in skeletal muscle and adipose tissue and to some extent in brain and liver. Several suggestions have been made for the physiological role of CA III, but its function remains uncertain (*7*, *9*, *10*). HCA III is different from other catalytic isozymes in the α class because of its resistance to sulfonamide inhibitors and lower catalytic activity. HCA III has values of k_{cat} and k_{cat}/K_m for hydration of CO_2 near 2 ms^{-1} and 0.3 μM^{-1} s^{-1} compared with maximal values near 10^3 ms^{-1} and 100 μM^{-1} s^{-1} for HCA II (*1*−*3*, *11*, *12*). The crystal structures of bovine CA III (BCA III) (*13*) and rat CA III (RCA III) (*14*) have been previously determined at 2.0 and 1.8 Å resolution, respectively, and are extremely similar in backbone and side chain conformation.

A key to understanding the differences in catalysis between CA II and CA III is residue 198, the side chain of which is located on the hydrophobic side of the active site cavity. These two isozymes have very similar backbone conformations (*13*). In HCA III, Phe 198 has its phenyl ring about 5 Å from the zinc; in HCA II this site is occupied by leucine. There is about a 10-fold enhancement in both k_{cat} and k_{cat}/K_m replacing Phe 198 with Leu in HCA III (*12*). Interestingly, there is very little change in catalysis for the reverse replacement; the mutant L198F HCA II has catalytic activity very similar to that of HCA II (*15*). There is an increase in

[†] This work was supported by a grant from the National Institutes of Health (GM25154) and by the Thomas Maren Foundation.

[‡] The atomic coordinates have been deposited in the Protein Data Bank (entries 1Z93 and 1Z97).

* To whom correspondence should be addressed. R.M.: phone, (352) 392-5696; fax, (352) 392-3422; e-mail, rmckenna@ufl.edu. D.N.S.: phone, (352) 392-3556; fax, (352) 392-9696; e-mail, silvermn@college.med.ufl.edu.

[§] Department of Biochemistry and Molecular Biology.

[||] Department of Pharmacology and Therapeutics.

[1] Abbreviations: HCA III, isozyme III of human carbonic anhydrase; F198L HCA III, the site-specific mutant of human carbonic anhydrase III in which Phe 198 is replaced with Leu; RCA III, rat carbonic anhydrase III; PEG, poly(ethylene glycol); rms, root mean squared; 4-MI, 4-methylimidazole.

10.1021/bi050610h CCC: $30.25 © 2005 American Chemical Society
Published on Web 07/07/2005

the pK_a of the zinc-bound water from a value of <6 in wild-type HCA III to 6.9 in F198L HCA III (*16*). This enhancement was suggested to be due to an altered interaction in F198L HCA III between the side chain of Thr 199 and the zinc-bound solvent molecule (*17*). The side chain of Thr 199 is a hydrogen bond acceptor for the zinc-bound water.

In HCA II the side chain of His 64 acts as a proton shuttle group (*1*−*5*). HCA III has a lysine at residue 64 which is not efficient in proton transfer during catalysis; this accounts in part for the lower catalytic turnover for this isozyme (*12*). However, the catalytic activity can be enhanced by the presence of proton donors from solution. There are numerous studies of the activation by exogenous proton donors of the hydration of CO_2 catalyzed by carbonic anhydrases (*8*, *18*−*20*). In this capacity, imidazole and derivatives in solution are second substrates that carry out the function of the proton acceptor B in eq 2. Mutants of HCA II lacking the proton shuttle His 64 are activated nearly to the level of catalytic activity of wild type by millimolar concentrations of imidazole and derivatives (*8*, *18*, *19*). The observation that the rescued activity near saturating concentrations of imidazole is close to that of wild type suggests that the rescuing imidazole binds in a region close to the side chain of His 64 in HCA II or the imidazole binds elsewhere in the active site cavity, and the great flexibility of water structures produces a pathway for proton transfer about equivalent energetically to His 64. Hence, there is interest in identifying binding sites for these rescue agents. Despite considerable study, there is little structural information on the binding sites from which this activation occurs. X-ray crystallography identified two binding sites for 4-methylimidazole (4-MI) in the active site of H64A HCA II (*18*, *21*) and for histamine in the active site of HCA II (*22*). It was determined that the binding site of 4-MI associated with the indole ring of Trp 5 is nonproductive in proton transfer (*19*).

We report the crystal structures of C-terminal hexahistidine-tagged HCA III and F198L HCA III and the enhancement of catalytic activity by exogenous proton donors containing imidazole rings. These studies imply that the phenyl side chain of Phe 198 in HCA III is a steric constriction in the active site but can also function as a binding site for the activation of catalysis by histidylhistidine.

EXPERIMENTAL PROCEDURES

Enzymes. We prepared C183S-C188S HCA III with a hexahistidine tail at the C-terminus. The mutations at positions 183 and 188 were to enhance crystallization by removing oxidizable cysteine residues and the hexahistidine tail to facilitate purification. The positions of residues 183 and 188 are solvent exposed on the side of the enzyme opposite to the active site. The mutations C183S and C188S and the presence of the hexahistidine tail did not affect catalysis. The expression, crystallization, data collection, molecular replacement, and initial phasing of the C183S-C188S HCA III structure with a C-terminal hexahistidine tag (referred to as HCA III in this paper) have been previously reported (*23*) and therefore will be discussed only briefly. Expression of HCA III was carried out using *Escherichia coli* BL21(DE3)pLysS (*24*). Protein purification was achieved by immobilized metal affinity chromatography (Ni-NTA; Qiagen), taking advantage of the exposed C-terminal hexahistidine tag. A further purification step involved anion-exchange chromatography prior to protein concentration and crystallization. Expression and purification of F198L-C183S-C188S HCA III (referred to as F198L HCA III for the remainder of the text) were performed in a manner similar to that of HCA III. Concentrations of HCA III and F198L HCA III were determined from the molar extinction coefficient 6.2×10^4 M^{-1} cm^{-1} at 280 nm (*25*).

Crystallography. Diffraction quality crystals of HCA III and F198L HCA III were obtained by the hanging-drop vapor diffusion method (*26*) using a 6.7 and 6.0 mg/mL enzyme solution, respectively. Prior to crystallization the enzyme was buffered in 10 mM Tris buffer, pH 8.0 for HCA III and pH 9.2 for F198L HCA III. Crystallization drops of HCA III were obtained by mixing 10 μL of enzyme solution with 3 μL of precipitant solution (30% PEG 8K/10 mM Tris, pH 8.0). This procedure was the same for F198L HCA III except that 10 μL of enzyme solution was mixed with 5 μL of precipitant solution (30% PEG 8K/10 mM Tris, pH 9.2). Both drops were suspended over 1 mL of their respective precipitant solution.

Sixty degrees of data were collected from a single crystal of HCA III, and 147 degrees of data were collected from two crystals of F198L HCA III using an R-axis IV++ image plate system with Osmic mirrors and a Rigaku HU-H3R CU rotating anode operating at 50 kV and 100 mA with a crystal-to-detector distance of 150 mm and a 0.5° and 1.0° oscillation angle, respectively. The HCA III data were collected at 293 K with an exposure time of 60 s per frame while F198L HCA III data was collected at 100 K with an exposure time of 300 s per frame. The F198L HCA crystals were quick-dipped into a cryoprotectant solution (30% glycerol in precipitant solution) prior to flash freezing. Both data sets were indexed, scaled, and reduced with the software DENZO and SCALEPACK (*27*). The HCA III data set was assigned the hexagonal space group $P6_5$ with unit cell parameters a = 44.7 Å and c = 222.2 Å resulting in an R_{sym} of 10.2% (32.4% outer resolution shell) and overall completeness of 88.1% (85.0% outer resolution shell) to 2.1 Å resolution. The F198L HCA III data were assigned in the monoclinic space group $P2_1$ with unit cell parameters a = 44.5 Å, b = 70.8 Å, and c = 44.5 Å and β = 115.1 ° resulting in an R_{sym} of 8.1% (34.1% outer resolution shell) with an overall completeness of 92.3% (87.7% outer resolution shell) also to 2.1 Å resolution (Table 1).

Phasing and initial refinement of HCA III were performed by molecular replacement methods using the 1.8 Å resolution model of RCA III as the search model (*14*). The results of the rotation and translation searches have been previously described for HCA III by Duda et al. (*23*). Similar methods were employed to phase the F198L HCA III data, using the solved HCA III model (with residue 198 mutated to an alanine to prevent any phase bias), which was placed into the monoclinic $P2_1$ space group using the rotation and translation matrix obtained from the software CNS (*28*). An initial phasing data set was generated by rigid-body refinement resulting in an R_{work} of 29.1%.

Both structures were refined using standard protocols in CNS (*28*). After one cycle of rigid-body refinement followed by geometry-restrained positional refinement and placement of the zinc ion, a cycle of simulated annealing, refined by heating to 3000 K and gradual cooling, was carried out. A

Table 1: Crystallographic Statistics

	HCA III	F198L HCA III
	Data Collection	
resolution (Å)	20.0−2.10 (2.17−2.10)[a]	20.0−2.10 (2.17−2.10)[a]
space group	$P6_5$	$P2_1$
unit cell (Å)/°	$a = b = 44.7$, $c = 222.2$	$a = 44.5$, $b = 70.8$, $c = 44.5$, $\beta = 115.1°$
molecules/asu	1	1
R_{sym}[b] (%)	10.2 (32.4)	8.1 (34.1)
unique reflections	12938	13525
completeness (%)	88.1 (85.0)	92.3 (87.7)
	Refinement	
protein atoms	2127	2124
water molecules	109	98
	Average *B* Factors (Å^2)	
protein main chain	29.9	24.7
protein side chain	31.7	26.7
solvent molecules	39.0	29.6
Luzzati coord error (Å)	0.3	0.3
R_{cryst}[c]/R_{free}[d] (%)	20.5/25.8	18.6/23.7
rmsd bond lengths (Å)/ angles (deg)	0.006/1.4	0.006/1.3

[a] Data for the highest resolution shell are given in parentheses. [b] $R_{sym} = (\sum|I - \langle I\rangle|/\sum I) \times 100$, where I is the intensity of a reflection and $\langle I\rangle$ is the average intensity. [c] $R_{cryst} = (\sum_{hkl}|F_o - KF_c|/\sum_{hkl}|F_o|) \times 100$. [d] R_{free} is calculated from 5% randomly selected data for cross-validation.

cycle of temperature factor refinement and energy minimization resulted in an R_{work} of 24.2% for HCA III and 23.9% for F198L HCA III. Interactive modeling building, using the graphics program O, version 7 (*29*), allowed for further improvement of the structures. Calculated $2|F_o| - |F_c|$ and $|F_o| - |F_c|$ electron density maps contoured at 2σ showed electron density for the extending C-terminus for both structures. For both HCA III and F198L HCA III all six histidine residues of the C-terminal His tag were built, and the side chains could be placed. After additional cycles of refinement and interactive building and solvent placement, the final statistics for the HCA III structure were R_{cryst} of 20.5% and R_{free} of 25.8% and for F198L HCA III were R_{cryst} of 18.6% and R_{free} of 23.7% (Table 1).

^{18}O Exchange. Membrane-inlet mass spectrometry was used to measure the exchange of ^{18}O between CO_2 and water at chemical equilibrium catalyzed by carbonic anhydrase (*20*, *30*) (eqs 3 and 4). We used an Extrel EXM-200 mass

$$HCOO^{18}O^- + EZnH_2O \leftrightharpoons EZnHCOO^{18}O^- \leftrightharpoons COO + EZnO^{18}H^- \quad (3)$$

$$EZnO^{18}H^- + BH^+ \leftrightharpoons EZnH_2{}^{18}O + B \overset{H_2O}{\rightleftharpoons} EZnH_2O + H_2{}^{18}O + B \quad (4)$$

spectrometer with a membrane-inlet probe (*30*) to determine the isotopic content of CO_2. Solutions contained a 25 mM total concentration of all species of CO_2 unless otherwise indicated.

This method gives two rates for the ^{18}O exchange catalyzed by carbonic anhydrase (*30*). The first is R_1, the rate of exchange of CO_2 and HCO_3^- at chemical equilibrium, as shown in eq 5. Here k_{cat}^{ex} is a rate constant for maximal

$$R_1/[E] = k_{cat}^{ex}[S]/(K_{eff}^{S} + [S]) \quad (5)$$

interconversion of substrate and product, K_{eff}^{S} is an apparent binding constant for substrate to enzyme, and [S] is the concentration of substrate, either CO_2 or bicarbonate (*30*−*32*). The ratio k_{cat}^{ex}/K_{eff}^{S} is, in theory and in practice, equal to k_{cat}/K_m obtained by steady-state methods.

This method also determines R_{H_2O}, the rate of release from the enzyme of water bearing substrate oxygen (eq 4). This is the component of the ^{18}O exchange that is enhanced by exogenous proton donors. In such enhancements, the exogenous donor acts as a second substrate in the catalysis providing a proton (eq 4), and the resulting effect on ^{18}O exchange is described by eq 6. In eq 6, k_B^{obs} is the observed

$$R_{H_2O}/[E] = k_B^{obs}[B]/(K_{eff}^{B} + [B]) + R_{H_2O}{}^0/[E] \quad (6)$$

maximal rate constant for the release of $H_2{}^{18}O$ to bulk water caused by the addition of the buffer. K_{eff}^{B} is an apparent binding constant of the buffer to the enzyme, [E] and [B] are the concentrations of total enzyme and total buffer, and $R_{H_2O}{}^0$ is the rate of release of $H_2{}^{18}O$ into solvent water in the absence of buffer and represents the contribution to proton transfer from other sites on the enzyme or possibly solvent water itself.

RESULTS

Structure. The structures of HCA III and F198L HCA III, each exhibiting an ordered C-terminal hexahistidine extension, have been solved and refined to 2.1 Å resolution (Table 1). Analysis of the bond geometry of the two structures, using the software package PROCHECK (*33*), showed them to conform to standard values. The estimated upper error limit for the atomic coordinates of both HCA III and F198L HCA III was 0.3 Å based on Luzzati analysis (*34*) (Table 1). The structures of these two enzymes are highly superimposable with rms deviation of all atoms at 0.4 Å, excluding residue 198. For each enzyme, HCA III and F198L HCA III, the hexahistidine tag at the C-terminal end of the protein extends from the back side of the enzyme, on the side of the enzyme that is opposite to the active site cavity. In the crystal structures, there is no interaction of this hexahistidine tag with any residues of the active site cavity of the same enzyme (Figure 1). However, inspection of the $2|F_o| - |F_c|$ and $|F_o| - |F_c|$ electron density maps for HCA III and F198L HCA III revealed the ordered C-terminal extension of residues 262−267 of the hexahistidine tag located in the active site cavity of an adjacent symmetry-related molecule in both the $P6_5$ (HCA III) and $P2_1$ (F198L HCA III) space groups, respectively (Figure 1C,D). Comparisons of the structure of this hexahistidine-tagged HCA III with reported structures of BCA III (*13*) and RCA III (*14*) suggested that the presence of hexahistidine in the active site cavity caused no significant changes in the structure of the enzyme (Supporting Information S1).

The general conformation, positioning, and interactions of the hexahistidine extensions in the active site cavity of HCA III and F198L HCA III were similar, surprising considering the different packing arrangements in the two crystal systems (Figure 1). There were several conserved H-bond interactions between backbone carbonyl oxygens of the hexahistidine extensions and active site side chains (these included the backbone carbonyl oxygens of His 263 and His

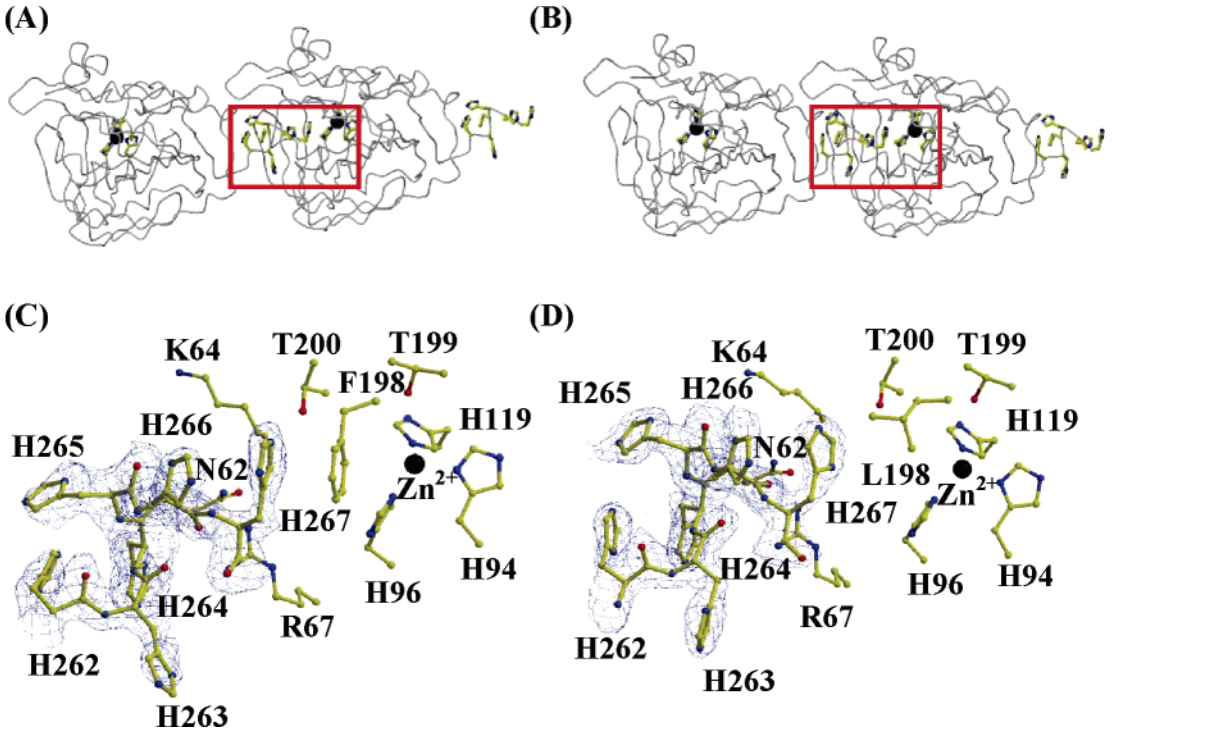

FIGURE 1: C-Terminal hexahistidine tag (262−267) interactions. Packing diagram depicting a reference CA III and the unit cell translated related molecule (1,0,0) with its hexahistidine tag buried within the active site of the reference molecule. (A) HCA III and (B) F198L HCA III in $P6_5$ and $P2_1$ space groups, respectively. The active site histidines, zinc ion, and heaxahistidine tag are depicted as ball-and-stick models. The red open box depicts a close-up view of the hexahistidine tag in the active site of (C) HCA III and (D) F198L HCA III. The $2|F_o - F_c|$ electron density for the hexahistidine tag is colored blue and contoured at 1σ. All residues are as labeled. Figure generated and rendered using BobScript and Raster3D (*46*, *47*).

266 with Arg 67, and His 267 and Arg 91) and several conserved hydrophobic contacts (these included the imidazole ring of His 263 with Val 69, and His 267 with Phe 131) for both structures. Interestingly, in the HCA III structure, the imidazole ring of His 267 formed an additional π-stacking interaction with the phenyl ring of Phe 198 (absent in F198L HCA III) and also made additional hydrophobic contacts with residues Pro 202 and Glu 204. Other additional hydrophobic interactions of the hexahistidine tag in HCA III were the imidazole rings of His 263 and His 264 with Leu 60. On the other hand, the hexahistidine tag in F198L HCA III exhibited additional H-bond interactions between the backbone carbonyl oxygens of His 264 with Asn 62 and His 266 with Gln 92, and two solvent molecules (not observed in HCA III) further stabilized the carbonyl oxygens of His 264 and His 267. It was also observed, for both hexahistidine tags, that there were no observable interhexahistidine interactions, yet they both had the same overall conformation, induced most likely by the structural constraint imposed by the enzyme active sites. In the case of HCA III there was a general trend of more hydrophobic contact stability, whereas in the F198L HCA III there was a trend of more polar interactions (Figure 1, Supporting Information S2).

Lysine 64 in HCA III is a residue of interest since this is the position from which His 64 acts as a proton shuttle in the more efficient CAs of the α class (*5*). In crystal structures of HCA II, His 64 is in two stable conformers, an "in" orientation extending toward and an "out" orientation pointing away from the active site zinc, with both conformations having no apparent interactions with other residues (*6*, *35*). The structure of HCA III revealed that the Nζ nitrogen of Lys 64 is hydrogen-bonded (2.9 Å) to the backbone carbonyl

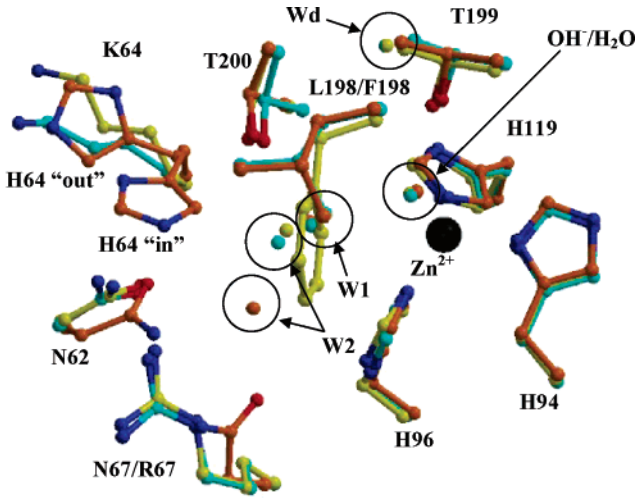

FIGURE 2: Superimposition of the active sites of HCA II, HCA III, and F198L HCA III. HCA II is in orange (histidine 64 side chain shown in the "in" and the "out" conformation, as labeled). HCA III and F198L HCA III are shown in yellow and cyan, respectively. Conserved solvent molecules (zinc-bound hydroxide/water, W1, W2, and Wd) assigned to each structure, HCA II, HCA III, and F198L HCA III, are colored orange, yellow, and cyan, respectively. Note the open circles illustrating the conservation of the solvent network (with the exception of W2 in the case of HCA II). Figure generated and rendered using BobScript and Raster3D (*46*, *47*).

of Trp 5 and points away from the active site (Figure 2, Supporting Information S3). Interestingly, a different interaction of Lys 64 was observed for BCA III in which the side chain forms a salt bridge with Glu 4 (*13*). The side chain of Lys 64 in F198L HCA III adopts yet a different conformation than that observed in either HCA III or BCA III. In this case

the Nζ nitrogen has no apparent interactions with other amino acids and is 12.5 Å from the zinc ion, somewhat closer than 13.5 Å seen for HCA III but still pointing out of the active site (Figure 2, Supporting Information S3). This difference in the observed side chain conformations of Lys 64 may be due to the difference in crystallization conditions (HCA III and F198L HCA III crystallized at pH 8.0 and 9.2, respectively), yet in all cases the lysine points away from the active site.

Another residue important in the catalysis is Thr 199, the side chain hydroxyl of which is a hydrogen bond acceptor for the zinc-bound solvent (*1*−*2*). The distances between Thr 199 Oγ1 and the oxygen of the zinc-bound solvent molecule were the same within error for HCA III, RCA III, and HCA II (2.5 Å) but somewhat larger for F198L HCA III (2.8 Å) (Figure 2, Supporting Information S3). Analyses of the distances between the Cγ atom of either Leu 198 or Phe 198 and the zinc ion, the zinc-bound solvent molecule, W1, W2, and Wd (Figure 2) are provided in Supporting Information S1. The Cγ atom was chosen for this analysis due to its central location on the side chains of both Leu and Phe. The Cγ atom for Leu 198 in F198L HCA III was 7.8 Å from the zinc, greater than for HCA III in which this distance is 7.1 Å.

Ordered Solvent. Comparison of the positions of ordered solvent molecules in HCA III and F198L HCA III revealed an overall conservation of several solvent molecules, despite the bound hexahistidine tag; these included the zinc-bound hydroxide/water, W1, W2, and Wd (known as "deep water") shown in Figure 2. These solvent locations had been previously observed in RCA III (*14*) and HCA II (*35*, *36*). The solvent molecule W2 was slightly displaced in the CA III structures compared to HCA II, mostly likely a consequence of the side chain of Lys 64 in HCA III compared with His 64 in HCA II (Figure 2). Previously, Eriksson and Liljas, when describing the structure of BCA III, referred to a water molecule hydrogen-bonded to the π-ring of Phe 198 (*13*); in the HCA III structure described in this work, no such water molecule was observed and was most likely displaced by the binding of the hexahistidine extensions into the active sites.

Catalysis. The catalytic properties of F198L HCA III compared with HCA III in the hydration of CO_2 and in the exchange of ^{18}O between CO_2 and water have been reported by LoGrasso et al. (*16*). The maximal, pH-independent values of the steady-state constants k_{cat} and k_{cat}/K_m for hydration of CO_2 and R_{H_2O} for the catalyzed ^{18}O exchange are given in Table 2. These data show an increase by at least 10-fold in catalytic activity resulting from the replacement of Phe 198 with Leu. Under our experimental conditions the values of the catalytic constants k_{cat}/K_m and R_{H_2O} in Table 2 were identical for HCA III and F198L HCA III with and without the hexahistidine extension.

Addition of imidazole enhanced the proton-transfer-dependent rate constant R_{H_2O}/[E] during catalysis by both HCA III and F198L HCA III (Figure 3), which is represented as k_B^{obs}/K_{eff}^B of eq 6 in Table 2. There was a greater enhancement observed for the mutant. As shown in Figure 3, saturation was not approached for F198L HCA III or HCA III even at 200 mM imidazole; hence, we were not able to determine K_{eff}^B or k_B^{obs} of eq 6. In catalysis by both HCA III and F198L HCA III there was no change upon increasing imidazole concentration on the rate constant R_1/[E]; this constant reports the interconversion of CO_2 and HCO_3^- (eq 5, data not shown; for F198L HCA III there was a very slight inhibition of about 20% at 200 mM imidazole; see Figure 3 of ref *16*).

Table 2: Maximal, pH-Independent Values of Steady-State Constants for Hydration of CO_2, Rate Constant R_{H_2O}/[E] for ^{18}O Exchange, and Apparent Second-Order Rate Constants for Activation of HCA III and F198L HCA III by Imidazole and Histidylhistidine

	HCA III	F198L HCA III
k_{cat}/K_m ($\mu M^{-1}\,s^{-1}$)[a]	0.3	7.4
k_{cat} (ms^{-1})[a]	2.0	22
R_{H_2O}/[E], no buffer (ms^{-1})[b]	1.8	20
k_B^{obs}/K_{eff}^B for imidazole ($\mu M^{-1}\,s^{-1}$)[b]	0.1	0.5
k_B^{obs}/K_{eff}^B for histidylhistidine ($\mu M^{-1}\,s^{-1}$)[c]	0.05	none
pK_a, zinc-bound H_2O[d]	<6.0	6.9

[a] These are maximal, pH-independent values of k_{cat}/K_m and k_{cat} for hydration of CO_2 at 25 °C from ref *16*. [b] Conditions as in Figure 3. [c] Conditions as in Figure 4. [d] From ref 16.

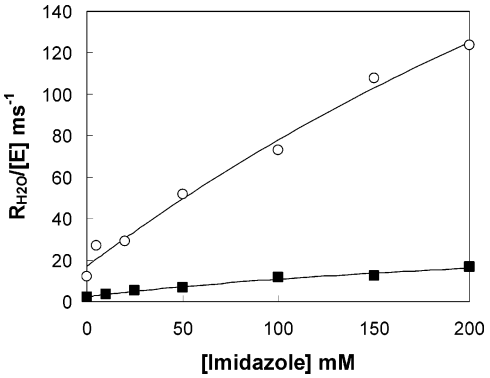

FIGURE 3: Activation by imidazole of R_{H_2O}/[E] catalyzed by (■) HCA III and (○) F198L HCA III. The pH was 7.3 for HCA III and 7.2 for F198L HCA III at 25 °C with the total ionic strength of the solution maintained at a minimum of 0.2 M by addition of Na_2SO_4. Data are from refs *16* and *19*. The solid lines are a fit of eq 6 to the data with parameters given in Table 2.

The dipeptide histidylhistidine was found to activate R_{H_2O}/[E] for HCA III; however, histidylhistidine had no measurable effect on catalysis by F198L HCA III (Figure 4, Table 2). It is interesting to note that increasing concentrations of histidylhistidine caused an inhibition in R_1/[E] for HCA III but not (or very slight) for F198L HCA III (Figure 4). This inhibition may arise by binding of histidylhistidine at the metal in a manner described for the binding of imidazole to HCA I (*37*) or for the binding of 4-methylimidazole to H64A HCA II (*38*). Another possibility is that histidylhistidine binds to the zinc through its carboxyl group. In either case, the data indicate that histidylhistidine is capable of binding deep in the active site cavity.

DISCUSSION

With the structural and kinetic data of this report, we are able to comment on two significant issues in catalysis by carbonic anhydrase. The first is the role of residue 198 as a significant contributor to the unique catalytic properties of HCA III among the carbonic anhydrases of the α class. The second is to find within the active site cavity locations from which proton transfer is efficient.

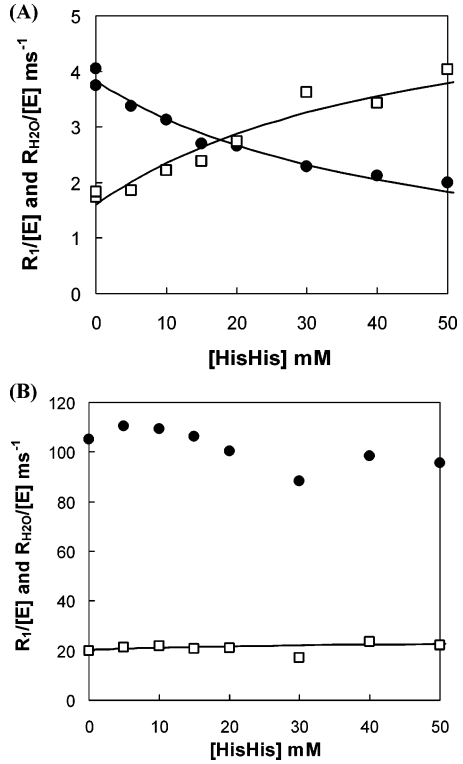

FIGURE 4: Effect of histidylhistidine (A) on (□) R_{H_2O}/[E] and (●) R_1/[E] catalyzed HCA III and (B) on (□) R_{H_2O}/[E] and (●) R_1/[E] catalyzed F198L HCA III. For both experiments the pH was 7.0 at 25 °C with the total ionic strength of the solution maintained at a minimum of 0.2 M by addition of Na_2SO_4. The solid lines are a fit of eq 6 to the data R_{H_2O}/[E] with parameters given in Table 2.

Catalytic Activity of HCA III. The catalytic activity of HCA III is considerably lower than that of HCA II in the hydration of CO_2 by at least 2 orders of magnitude (Table 2). A feature of the structure that is relevant in explaining the smaller activity of HCA III is the difference at position 198, which is Phe in HCA III and Leu in HCA II and other catalytic carbonic anhydrases of the α class. We examined the structures of HCA II, RCA III, HCA III, and F198L HCA III (Supporting Information S1). This reveals that the Cγ of Phe 198 in HCA III and RCA III is closer to the zinc by 0.5−0.7 Å than the Cγ of Leu 198 in F198L HCA III; all of these are considerably closer by 0.7−1.4 Å than the Cγ of Leu 198 in HCA II. This change in position of the side chain is not a consequence of a shift in backbone conformation; the distance from the Cα of residue 198 to the zinc is essentially the same at 6.7 and 6.9 Å for HCA III and F198L HCA III, respectively. Thus, not only is the active site of HCA III constrained by the presence of the bulkier phenyl ring, but the side chain has been brought closer to the zinc (Figure 2). This extra constraint on the active site of HCA III may be responsible for the lower catalytic activity k_{cat}/K_m than that for HCA II, which is near diffusion control at 100 μM^{-1} s^{-1} (*1*). It certainly also would explain the weaker binding of the classic carbonic anhydrase inhibitors acetazolamide and ethoxzolamide on wild-type HCA III compared with F198L HCA III (*16*).

Another structural difference is in the side chain conformation of Lys 64, which in F198L HCA III extends out of the active site cavity with no predominant interaction with other residues but in HCA III forms a hydrogen bond with the backbone carbonyl oxygen of Trp 5 (Supporting Information S3). Previous kinetic comparison of HCA III and K64A HCA III has shown that Lys 64 does not participate significantly in proton transfer (*20*), unlike His 64 in HCA II (*5*). Kinetic results suggested that the conformations available to Lys 64 are dependent on other residues of the active site cavity. For example, the replacement of Arg 67 with Asn in the active site cavity increased k_{cat} about 10-fold; Jewell et al. suggested that this is in part due to a role in proton transfer for Lys 64 in R67N HCA III which would have an increased range of side chain conformations in the absence of the charged Arg 67 side chain (*12*). These results with Lys 64 are reminiscent of similar results in which the side chain conformation of His 64 is altered in the mutant T200S HCA II compared with wild type (*39*). The authors suggested that the side chain orientation of His 64 depended on surrounding solvent structure that could be related to distant mutations within the active site cavity. Tu et al., using a double mutant cycle based on K64A-F198L HCA III, found that replacing Lys 64 with Ala and Phe 198 with Leu showed simple additive effects on k_{cat}/K_m for hydration and on the pK_a of the zinc-bound water, implying that these residues do not interact in the mutations studied (*40*). However, the different orientations of Lys 64 in Figure 2 may simply be a result of the more basic crystallization conditions for F198L HCA III (pH 9.2) compared with HCA III (pH 8.0), which would decrease ionization of Lys 64 Nζ in F198L HCA III releasing the side chain constraint.

Interaction of Thr 199 and Zinc-Bound Aqueous Ligand. The pH dependence of the catalytic activity k_{cat}/K_m for hydration of CO_2 catalyzed by carbonic anhydrase is determined predominantly by the pK_a of the zinc-bound water molecule (*1*). In mutants of HCA III containing replacements at position 198, this pK_a varied from <6.0 for wild type to 9.2 for F198D HCA III (*41*). The pK_a of the zinc-bound water was greater by nearly 1 pK_a unit for F198L HCA III compared with HCA III (Table 2). LoGrasso et al. found a correlation between hydrophobicity of the residue at position 198 and this pK_a (*41*). Part of the enhanced activity k_{cat}/K_m of F198L HCA III compared with wild type may be related to this pK_a in that correlations of the basicity of metal-bound hydroxides in nucleophilic attack on CO_2 are well documented (*42*). This emphasizes the strong influence of this position on the properties of the active site. Figure 2 showed that the replacement of Phe 198 with Leu in HCA III caused no backbone changes or changes in coordination to the metal and there is no alteration in the water structure, including the zinc-to-oxygen distance.

It has also been suggested that the increase in pK_a may be related to a change in distance or orientation between Thr 199 and the zinc-bound solvent molecule (*17*). On the basis of the double mutant F198L-T199A HCA III, Chen et al. (*17*) concluded that the enhancement in the pK_a of the zinc-bound water observed by the substitution of Phe 198 with Leu is consistent with an altered interaction of the adjacent Thr 199 with the zinc-bound solvent molecule. They observed that the enhancement in pK_a caused by the replacement of Phe 198 with Leu was abolished when Thr 199 was also replaced with Ala (*17*). The enhancement in activity of F198L HCA III compared with HCA III was associated with decrease in free energy $\Delta\Delta G$ from 1.4 to 1.9 kcal/mol. Also, the change in the pK_a of the zinc-bound water caused by the replacement of Phe 198 with Leu was

associated with a $\Delta\Delta G$ of 2.6 kcal/mol. Chen et al. (*17*) suggested that these changes caused by replacement of a phenylalanine to a leucine were due to a conformational change in the hydrogen bond interaction between the side chain of Thr 199 and the zinc-bound water. In the structure studies reported here, there does appear to be an increased distance of the hydrogen bond observed between T199 Oγ1 and the zinc-bound water (2.8 Å) compared with HCA III, RCA III, and HCA II (2.5−2.6 Å), tempered by the experimental uncertainties (0.3 Å) based on Luzzati analysis (*34*). The potential energy of a O−H···O hydrogen bond that is altered in distance by 0.2 Å can readily amount to as much as 2.0 kcal/mol (*43*). Within the experimental uncertainties, we conclude that a comparison of the crystal structures of HCA III and F198L HCA III is weakly supportive of, but at least does not exclude, an effect of Phe 198 on the interactions of the adjacent Thr 199 with the zinc-bound solvent molecule.

Activation of Carbonic Anhydrase. Previously, crystallographic studies have been used to identify binding sites of imidazole rings within the active site cavity of carbonic anhydrase. Different binding sites for histamine and phenylalanine were found within the active site cavity of HCA II (*22*, *44*). More recently, binding sites for 4-methylimidazole within the active site cavity of H64A HCA II have been found associated with the side chains of Trp 5 (*18*) and Glu 69 (*21*). The combination of these results suggests that many different binding sites may exist within the active site cavity of carbonic anhydrase for small, exogenous proton donors containing imidazole rings.

The hexahistidine extension on the C-terminal end of HCA III and F198L HCA III, useful in purification, is also useful in identifying binding sites of imidazole. These hexahistidine tails bind in the active site of the adjacent enzyme in the unit cell in the same mode and overall conformation for both structures, which is interesting given their two different space groups (Figure 1). The binding in the active site cavities of wild-type and F198L HCA III of the hexahistidine tails elucidates an array of possible binding sites for imidazole rings. However, there are specific interactions between the hexahistidine extensions and the active site cavities that differ between HCA III and F198L HCA III. Most notably, the imidazole ring of His 267 of the hexahistidine tag forms a π-stacking interaction with the phenyl ring of Phe 198 in HCA III, an interaction lacking in the mutant F198L HCA III. This observation suggests that imdazole can bind deep into the active site of HCA III, and this represents a previously unobserved, potentially productive binding site for imidazole in proton transfer (Figure 1). Such an interaction appears to be prominent in the activation of HCA III by histidylhistidine as demonstrated in the experiments of Figure 4. This dipeptide enhanced catalysis by HCA III in a manner suggesting activation of the proton-transfer pathway; that is, histidylhistidine enhanced R_{H_2O} catalyzed by HCA III in a saturable manner but not R_1, which showed some inhibition by histidylhistidine (Figure 4). This is the pattern found for activation of H64A HCA II by exogenous proton donors (*19*, *45*).

In a similar experiment, there was no activation of F198L HCA III upon addition of histidylhistidine (Figure 4). The data of Figure 4 suggest that the binding site for histidylhistidine is at Phe 198, perhaps in a manner similar to the binding of the hexahistidine tail. This site is not present in F198L HCA III and accounts for the lack of activation of catalysis by histidylhistidine. The phenyl ring of Phe 198 proposed as a binding site for histidylhistidine is about 5 Å from the zinc in HCA III. These results suggest that productive binding sites for activation of carbonic anhydrase could be closer to the zinc than the side chain of His 64 in HCA II, which in the "in" conformation is 7.5 Å from the zinc (*6*, *35*). In the case of activation by imidazole, which shows activation of both HCA III and F198L HCA III (Figure 3), the situation is more complex; that is, there is most likely an array of binding sites for imidazole that is different from that of histidylhistidine. The use of the hexahistidine extension and histidylhistidine has shown a likely site of activation of HCA III.

SUPPORTING INFORMATION AVAILABLE

The active site distance geometry of HCA III, F198L HCA III, RCA III, and HCA II (S1); the observed interactions between the hexahistidine tag in the active site of HCA III and F198L HCA III (S2); and the active sites of HCA III and F198L HCA III (S3). This material is available free of charge via the Internet at http://pubs.acs.org.

REFERENCES

1. Lindskog, S. (1997) Structure and mechanism of carbonic anhydrase, *Pharmacol. Ther. 74*, 1−20.
2. Christianson, D. W., and Fierke, C. A. (1996) Carbonic anhydrase: Evolution of the zinc binding site by nature and by design, *Acc. Chem. Res. 29*, 331−339.
3. Silverman, D. N., and Lindskog, S. (1988) The catalytic mechanism of carbonic anhydrase: Implications of a rate-limiting protolysis of water, *Acc. Chem. Res. 21*, 30−36.
4. Steiner, H., Jonsson, B.-H., and Lindskog, S. (1975) The catalytic mechanism of carbonic anhydrase. Hydrogen-isotope effects on the kinetic parameters of the human C isoenzyme, *Eur. J. Biochem. 59*, 253−259.
5. Tu, C. K., Silverman, D. N., Forsman, C., Jonsson, B. H., and Lindskog, S. (1989) Role of histidine 64 in the catalytic mechanism of human carbonic anhydrase II studied with a site-specific mutant, *Biochemistry 28*, 7913−7918.
6. Nair, S. K., and Christianson, D. W. (1991) Unexpected pH-dependent conformation of His-64, the proton shuttle of carbonic anhydrase II, *J. Am. Chem. Soc. 113*, 9455−9458.
7. Parkkila, S. (2000) An overview of the distribution and function of carbonic anhydrase in mammals, in *The Carbonic Anhydrases New Horizons* (Chegwidden, W. R., Carter, N. D., and Edwards, Y. H., Eds.) pp 79−93, Birkhäuser Verlag, Basel.
8. Sly, W. S., and Hu, P. Y. (1995) Human carbonic anhydrases and carbonic anhydrase deficiencies, *Annu. Rev. Biochem. 64*, 375−401.
9. Chegwidden, W. R., and Carter, N. D. (2000) Introduction to the carbonic anhydrases, in *The Carbonic Anhydrases New Horizons* (Chegwidden, W. R., Carter, N. D., and Edwards, Y. H., Eds.) pp 13−28, Birkhäuser Verlag, Basel.
10. Kim, G., Lee, T. H., Wetzel, P., Geers, C., Robinson, M. A., Myers, T. G., Owens, J. W., Wehr, N. B., Eckhaus, M. W., Gros, G., Wynshaw-Boris, A., and Levine, R. L. (2004) Carbonic anhydrase III is not required in the mouse for normal growth, development, and life span, *Mol. Cell. Biol. 24*, 9942−9947.
11. Sanyal, G. S., Swenson, E. R., Pessah, N. I., and Maren, T. H. (1982) The carbon dioxide hydration activity of skeletal muscle carbonic anhydrase. Inhibition by sulfonamides and anions, *Mol. Pharmacol. 22*, 211−220.
12. Jewell, D. A., Tu, C. K., Paranawithana, S. R., Tanhauser, S. M., LoGrasso, P. V., Laipis, P. J., and Silverman, D. N. (1991) Enhancement of the catalytic properties of human carbonic anhydrase III by site-directed mutagenesis, *Biochemistry 30*, 1484−1490.

13. Eriksson, A. E., and Liljas, A. (1993) Refined structure of bovine carbonic anhydrase III at 2.0 Å resolution, *Proteins: Struct., Funct., Genet. 16*, 29−42.
14. Mallis, R. J., Poland, B. W., Chatterjee, T. K., Fisher, R. A., Darmawan, S., Honztko, R. B., and Thomas, J. (2000) Crystal structure of S-glutathiolated carbonic anhydrase III, *FEBS Lett. 482*, 237−241.
15. Ren, X., Jonsson, B.-H., and Lindskog, S. (1991) Some properties of site-specific mutants of human carbonic anhydrase II having active-site residues characterizing carbonic anhydrase III, *Eur. J. Biochem. 201*, 417−420.
16. LoGrasso, P. V., Tu, C. K., Jewell, D. A., Wynns, G. C., Laipis, P. J., and Silverman, D. N. (1991) Catalytic enhancement of human carbonic anhydrase III by replacement of phenylalanine-198 with leucine, *Biochemistry 30*, 8463−8470.
17. Chen, X., Tu, C. K., LoGrasso, P. V., Laipis, P. J., and Silverman, D. N. (1993) Interaction and influence of phenylalanine-198 and threonine-199 on catalysis by human carbonic anhydrase III, *Biochemistry 32*, 7861−7865.
18. Duda, D., Tu, C. K., Qian, M., Laipis, P. J., Agbandje-McKenna, M., Silverman, D. N., and McKenna, R. (2001) Structural and kinetic analysis of the chemical rescue of the proton-transfer function of carbonic anhydrase II, *Biochemistry 40*, 1741−1748.
19. An, H., Tu, C. K., Duda, D., Montanez-Clemente, I., Math, K., Laipis, P. J., McKenna, R., and Silverman, D. N. (2002) Chemical rescue in catalysis by human carbonic anhydrases II and III, *Biochemistry 41*, 3235−3242.
20. Silverman, D. N., Tu, C. K., Chen, X., Tanhauser, S. M., Kresge, A. J., and Laipis, P. J. (1993) Rate-equilibria relationships in intramolecular proton transfer in human carbonic anhydrase III, *Biochemistry 32*, 10757−10762.
21. Duda, D., Govindasamy, L., Agbandje-McKenna, M., Tu, C. K., Silverman, D. N., and McKenna, R. (2003) The refined atomic structure of carbonic anhydrase II at 1.05 Å resolution: implications of chemical rescue of proton transfer, *Acta Crystallogr. D59*, 93−104.
22. Briganti, F., Mangani, S., Orioli, P., Scozzafava, A., Vernaglione, G., and Supuran, C. T. (1997) Carbonic anhydrase activators: X-ray crystallographic and spectroscopic investigations for the interaction of isozymes I and II with histamine, *Biochemistry 36*, 10384−10392.
23. Duda, D., Yoshioka, C., Govindasamy, L., An, H., Tu, C. K., Silverman, D. N., and McKenna R. (2002) Crystallization and preliminary X-ray analysis of human carbonic anhydrase III, *Acta Crystallogr. D58*, 849−852.
24. Studier, F. W., Rosenberg, A. H., Dunn, J. J., and Dubendorff, S. J. W. (1990) Use of T7 RNA polymerase to direct expression of cloned genes, *Methods Enzymol. 185*, 60−89.
25. Engberg, P., Millqvist, E., Pohl, G., and Lindskog, S. (1985) A comparison of the kinetic properties of native bovine muscle carbonic anhydrase and an activated derivative with modified thiol groups, *Arch. Biochem. Biophys. 241*, 628−638.
26. McPherson, A. (1982) *Preparation and Analysis of Protein Crystals*, Wiley and Sons, New York.
27. Otwinowski, Z., and Minor, W. (1997) Processing of X-ray diffraction data collected in oscillation mode, *Methods Enzymol. 276*, 307−326.
28. Brünger, A. T., Adams, P. D., Clore, G. M., DeLano, W. L., Gros, P., Grosse-Kuntsleve, R. W., Jiang, J. S., Kuszewski, J., Nilges, M., Pannu, N. S., Read, R. J., Rice, L. M., Simonson, T., and Warren, G. L. (1998) Crystallography and NMR system: A new software suite for macromolecular structure determination, *Acta Crystallogr. D54*, 905−921.
29. Jones, T. A., Zou, J. Y., Cowan, S. W., and Kjeldgaard, M. (1991) Improved methods for building protein models in electron density maps and the location of errors in these models, *Acta Crystallogr. A47*, 110−119.
30. Silverman, D. N. (1982) Carbonic anhydrase: oxygen-18 exchange catalyzed by an enzyme with rate-contributing proton-transfer steps, *Methods Enzymol. 87*, 732−752.
31. Simonsson, I., Jonsson, B.-H., and Lindskog, S. (1979) A ^{13}C nuclear-magnetic-resonance study of CO2−HCO3-exchange catalyzed by human carbonic anhydrase C at chemical equilibrium, *Eur. J. Biochem. 93*, 409−417.
32. Krebs, J. F., Ippolito, J. A., Christianson, D. W., and Fierke, C. A. (1993) Structural and functional importance of a conserved hydrogen bond network in human carbonic anhydrase II, *J. Biol. Chem. 268*, 27458−27466.
33. Laskowski, R. A., MacArthur, M. W., Moss, D. S., and Thornton, J. M. (1993) PROCHECK−a program to check the stereochemical quality of protein structures, *J. Appl. Crystallogr. 26*, 283−291.
34. Luzzati, V. (1952) Traitement statistique de erreurs dans la determination des structures cristallines, *Acta Crystallogr. 5*, 802−810.
35. Fisher, Z., Hernandez Prada, J. A., Tu, C., Duda, D, Yoshioka, C., An, H., Govindasamy, L., Silverman, D. N., and McKenna, R. (2005) Structural and kinetic characterization of active-site histidine as a proton shuttle in catalysis by human carbonic anhydrase II, *Biochemistry 44*, 1097−1105.
36. Håkansson, K., Carlsson, M., Svensson, L. A., and Liljas, A. (1992) Structure of native and apo carbonic anhydrase II and structure of some of its anion-ligand complexes, *J. Mol. Biol. 227*, 1192−1204.
37. Kannan, K. K., Petef, M., Fridborg, K., Cid-Dresdner, H., and Lovgren, S. (1977) Structure and function of carbonic anhydrases. Imidazole binding to human carbonic anhydrase B and the mechanism of action of carbonic anhydrases, *FEBS Lett. 73*, 115−119.
38. Elder, I., Tu, C. K., Ming, L. J., McKenna, R., and Silverman, D. N. (2005) Proton transfer from exogenous donors in catalysis by human carbonic anhydrase II, *Arch. Biochem. Biophys. 437*, 106−114.
39. Krebs, J. F., Fierke, C. A., Aleander, R. S., and Christianson, D. W. (1991) Conformational mobility of His-64 in the Thr-200- - -Ser mutant of human carbonic anhydrase II, *Biochemistry 30*, 9153−9160.
40. Tu, C. K., Chen, X., Ren, X., LoGrasso, P. V., Jewell, D. A., Laipis, P. J., and Silverman, D. N. (1994) Interactions of active-site residues and catalytic activity of human carbonic anhydrase III, *J. Biol.Chem. 269*, 23002−32006.
41. Lograsso, P. V., Tu, C. K., Chen, X., Taoka, S., Laipis, P. J., and Silverman, D. N. (1993) Influence of amino acid replacement at position 198 on catalytic properties of zinc-bound water in human carbonic anhydrase III, *Biochemistry 32*, 5786−5791.
42. Martin, R. B. (1976) Nucleophilicities of metal-ion bound hydroxide, *J. Inorg. Nucl. Chem. 38*, 511−513.
43. Jeffry, G. A. (1997) *An Introduction to Hydrogen Bonding*, Chapter 2, pp 11−32, Oxford University Press, Oxford.
44. Briganti, F., Scozzafava, A., and Supuran, C. T. (1999) Novel carbonic anhydrase isozymes I, II and IV activators incorporating sulfonyl-histamino moieties, *Bioorg. Med. Chem. Lett. 9*, 2043−2048.
45. Kresge, A. J., and Silverman, D. N. (1999) Application of Marcus rate theory to proton transfer in enzyme-catalyzed reactions, *Methods Enzymol. 308*, 276−297.
46. Merrit, E. A., and Bacon, D. J. (1997) Raster3D: Photorealistic Molecular Graphics, *Methods Enzymol. 277*, 505−524.
47. Esnouf, R. M. (1999) Further additions to MolScript version 1.4, including reading and contouring of electron-density maps, *Acta Crystallogr. D55*, 938−940.

BI050610H